

# The Proper Motion of the Central Compact Object RX J0822–4300 in the Supernova Remnant Puppis A

Werner Becker<sup>1,2</sup>, Tobias Prinz<sup>1</sup>, P. Frank Winkler<sup>3</sup>, Robert Petre<sup>4</sup>

## ABSTRACT

Using the High Resolution Camera (HRC) aboard the *Chandra* X-ray Observatory, we have re-examined the proper motion of the central compact object RX J0822–4300 in the supernova remnant Puppis A. New data from 2010 August, combined with three archival data sets from as early as 1999 December, provide a baseline of 3886 days (more than 10 1/2 years) to perform the measurement. Correlating the four positions of RX J0822–4300 measured in each data set implies a projected proper motion of  $\mu = 71 \pm 12 \text{ mas yr}^{-1}$ . For a distance of 2 kpc this proper motion is equivalent to a recoil velocity of  $672 \pm 115 \text{ km s}^{-1}$ . The position angle is found to be  $244 \pm 11$  degrees. Both the magnitude and direction of the proper motion are in agreement with RX J0822–4300 originating near the optical expansion center of the supernova remnant. For a displacement of  $371 \pm 31$  arcsec between its birth place and today’s position we deduce an age of  $(5.2 \pm 1.0) 10^3$  yrs for RX J0822–4300. The age inferred from the neutron star proper motion and filament motions can be considered as two independent measurements of the same quantity. They average to  $4450 \pm 750$  yrs for the age of the supernova remnant Puppis A.

*Subject headings:* stars: neutron - pulsars: individual: RX J0822–4300 - X-rays: stars

## 1. Introduction

There has long been broad consensus that core-collapse supernovae—the explosions of massive progenitors that produce Types II, Ib, and Ic events at least—leave behind a

---

<sup>1</sup>Max-Planck Institut für extraterrestrische Physik, Giessenbachstrasse 1, 85741 Garching, Germany

<sup>2</sup>Max-Planck Institut für Radioastronomie, Auf dem Hügel 69, 53121 Bonn, Germany

<sup>3</sup>Department of Physics, Middlebury College, Middlebury, VT 05753

<sup>4</sup>NASA Goddard Space Flight Center, Greenbelt, MD 20771

compact stellar remnant: either a neutron star or a black hole. Numerous central compact objects (CCOs) have been found within supernova remnant (SNR) shells (cf. Becker 2010 for a review), including near the centers of all three of the “oxygen-rich” SNRs (those with optical filaments dominated by ejecta that stem only from core-collapse supernovae) in the Galaxy: Cas A (Tananbaum 1999; Chakrabarty et al. 2001), Puppis A (Petre et al. 1996), and G292.0+1.8 (Hughes et al. 2001; Camilo et al. 2002).

Observations of proper motions for these CCOs, and of the ejecta-dominated filaments, provide the opportunity to investigate the dynamics of core-collapse explosions, as imprinted on the compact remnant and the ejecta. Anisotropies and/or bipolar jets appear typical of the ejecta distribution from core-collapse explosions. These are predicted from two- and three-dimensional models for core-collapse SNe (e.g., Burrows et al. 1995; Scheck et al. 2004, 2006; Wongwathanarat et al. 2010), and have been observed in all three of the Galactic oxygen-rich remnants. Asymmetries in the ejecta distribution are closely linked to the recoil of a CCO through conservation of momentum: if the explosion expels ejecta preferentially in one direction, the CCO must recoil in the opposite direction. One expects this recoil to be particularly apparent in Puppis A, where Winkler et al. (1988) found that all the visible ejecta knots are moving generally toward the north and east.

Following the discovery of RX J0822–4300 near the center of Puppis A (Petre et al. 1996), measuring its proper motion and recoil velocity was of obvious interest, and observations with this goal were carried out early in the *Chandra* mission. We have previously done two independent studies of the proper motion of RX J0822–4300 in a pair of papers: Hui & Becker (2006), henceforth HB06, and Winkler & Petre (2007), henceforth WP07. Both these papers were based on the same three epochs of data from the *Chandra* HRI over the 5.3-year period 1999 December–2005 April, and both measured a motion to the southwest, as expected, but with surprisingly high velocity: HB06 measured  $\mu = 107 \pm 34 \text{ mas yr}^{-1}$ , while WP07 found  $165 \pm 25 \text{ mas yr}^{-1}$ , corresponding to a transverse velocity of  $1122 \pm 327 \text{ km s}^{-1}$ , or  $1570 \pm 240 \text{ km s}^{-1}$ , respectively, if we take Puppis A’s distance as 2 kpc. Both these values are large compared with the typical birth velocities for pulsars of  $\sim 500 \text{ km s}^{-1}$  (Caraveo 1993; Frail et al. 1994; Hobbs et al. 2005). Furthermore, a recoil velocity much larger than  $1000 \text{ km s}^{-1}$  challenges models for producing pulsar kicks. Therefore, we have undertaken this joint follow-up study, taking advantage of *Chandra*’s unique spatial resolution with a time baseline twice as long as for our previous measurements.

## 2. Observations and Data Reduction

During the course of the *Chandra* mission, RX J0822–4300 has been observed on four occasions with the High Resolution Camera (HRC), the first of these in 1999 December. The first three observations have been already archived for several years. Because of the importance of RX J0822–4300 and the somewhat discrepant results found by HB06 and WP07, a new observation was proposed and carried out 2010 August 10–11. The new observation was carried out as two consecutive ObsIDs, with exposure times of  $\sim 40$  and  $\sim 38$  ks, with no intervening repointing, so they we have merged the event data for these in our analysis, for a total exposure of 78.9 ks. All observations are summarized in Table 1.

We downloaded fresh copies of the archived observations, and have reprocessed the events using the `chandra_repro` script. This and all subsequent analysis has been carried out using CIAO 4.4, and CALDB 4.4.8 to ensure that the latest corrections have been applied uniformly.

At the  $\sim 2$  kpc distance of Puppis A, a  $1000 \text{ km s}^{-1}$  transverse velocity of RX J0822–4300 would result in a proper motion of only  $\sim 0.1'' \text{ yr}^{-1}$ . Even for *Chandra*, whose absolute aspect resolution<sup>1</sup> is  $\sim 0''.6$ , the measurement of such a small proper motion is a challenge. Fortunately, there are three nearby X-ray sources whose positions are very well determined, since all correspond to optical stars in the UCAC3 (Zacharias et al. 2009) and 2MASS (Cutri et al. 2003) catalogs. Both HB06 and WP07 used these stars for astrometric correction in their analysis of the 1999–2005 data. We summarize their properties in Table 2 using the same nomenclature as in HB06. All three sources are detected with high significance in the 2010 observation. Using `wavedetect` we determined their position and count rates, including those of RX J0822–4300, as listed in Table 3. An image depicting their locations relative to RX J0822–4300 is shown in Fig. 1.

In order to achieve the highest accuracy in measuring the proper motion of RX J0822–4300, we followed the method described in §3.4 of WP07 with some improvements: we first measured the X-ray positions of RX J0822–4300 and the reference stars A, B, and C in each of the three archival datasets and in the 2010 observation (§2.1). The X-ray and optical positions of the stars were then used to transform the respective images of each observation to an absolute reference frame (§2.2). This procedure is necessary in order to include the HRC-S observation into our analysis, as there are small systematic effects and offsets in the rotation between the HRC-I and HRC-S detectors (WP07). The transformation coefficients determined this way were then used to derive the position of the neutron star

---

<sup>1</sup><http://cxc.harvard.edu/cal/ASPECT/celmon/>

at the corresponding epoch. We calculate the error budget exactly, rather than use the approximate method of WP07, which leads to somewhat larger errors for the corrected X-ray positions of RX J0822–4300 in the 1999 – 2005 data when compared to their work.

## 2.1. Spatial Analysis

In order to determine the position of the three reference stars and RX J0822–4300 we first generated a point-spread function (PSF) for every source in each of the four observations. This is required as the PSF broadens for sources at larger off-axis angles, leading to a larger position uncertainty when using the `wavedetect` tool. These positions were then used as input to *ChaRT*,<sup>2</sup> which computed the PSF for a point source at any off-axis angle. The computations were performed by generating 10 rays  $\text{mm}^{-2}$  for a peak energy of either 1.5 keV (WB & TP, the same as used by HB06) or 1.0 keV (FW, as in WP07); the resulting PSFs are virtually identical. The rays were then projected onto the HRC detector using *Marx*<sup>3</sup> to create an image of the PSF.

We obtained best-fit positions for all three reference stars and for RX J0822–4300 at each of the epochs using *Sherpa*, *Chandra*’s modeling and fitting package.<sup>4</sup> We followed the *Sherpa* thread “Accounting for PSF Effects in 2D Image Fitting,” in which a simulated PSF is convolved with an assumed source model to produce the best fit to the actual observational data. For each of the sources, we used a 2-D Gaussian model whose width was fixed at a small value – in most cases equal to the bin size used in the images – so that small intrinsic fluctuations in different PSFs and in the data did not lead to divergence. In our independent analyses, we used binnings of  $0.5 \times 0.5$  and  $1 \times 1$  pixel for RX J0822–4300, and  $1 \times 1$  and  $2 \times 2$  pixels for stars A, B, and C. In each case a PSF was constructed with *Marx* to match the bin size for the data. Because of the relatively low count rates for the three reference stars, we used the C-statistic to measure the goodness of fit. To obtain uncertainties, we used the *Sherpa* procedure `reg_proj` to map out  $1\sigma$ , 90%-confidence, and  $2\sigma$  contours in  $(x, y)$  detector coordinates. In every case, the best fits obtained with different binning choices were consistent, but smaller bin sizes generally gave somewhat smaller uncertainties.

Early in our data analysis we found a subtle software bug in the *Sherpa* package for CIAO version 4.3. By default *Sherpa* was using the brightest pixel in the PSF-image as

---

<sup>2</sup>*Chandra* Ray Tracer, <http://cxc.harvard.edu/chart/index.html>

<sup>3</sup><http://space.mit.edu/CXC/MARX/>

<sup>4</sup><http://cxc.harvard.edu/sherpa/>

the reference point for the convolution, regardless of the PSF-input-position specified to the task at the command line. For near on-axis sources, the brightest pixel is always very close to the nominal PSF center, but there can be significant displacements for a source that is a few arcminutes off-axis, with direction differences that depend on roll angle. This bug appears to be a long-standing one, and was apparently at work in the analysis reported in WP07, for two of us (WB & TP) were able to approximately reproduce those results for the 1999 – 2005 data. (HB06 used a different approach that did not involve PSF fits, so the result they reported was not affected.)

The *Chandra* Help Desk was able to identify this bug and eventually provided us with a workaround.<sup>5</sup>, which WB & TP have then used for all subsequent analysis. This workaround has been incorporated into CIAO version 4.4, which PFW has used to give essentially identical results. There are other differences between both the 2006-07 analyses and the present one that relate to the data themselves. Subsequent to the earlier analyses, there has been a complete reprocessing of all the *Chandra* data. Differences include use of improved aspect files and updated values for the degap corrections, detector gain, and the telescope effective focal length. As noted earlier, the present analysis has incorporated all the current wisdom regarding telescope and instrument performance.

The fitted X-ray positions of RX J0822–4300 (labeled as NS) and that of the three fiducial reference stars are listed for each of the four observations in Table 3, along the respective HRC counting rates.

## 2.2. Transformation to the World Coordinate System (WCS)

In order to determine the position of RX J0822–4300 relative to the three reference stars we assume a linear transformation with four free parameters: translations in Right Ascension,  $t_{RA}$ , and in Declination,  $t_{Decl}$ , a scale factor  $r$ , and a rotation of the detector  $\theta$ . The transformation can be expressed in the following way:

$$\begin{pmatrix} x_A & -y_A & 1 & 0 \\ y_A & x_A & 0 & 1 \\ x_B & -y_B & 1 & 0 \\ y_B & x_B & 0 & 1 \end{pmatrix} \begin{pmatrix} r \cos \theta \\ r \sin \theta \\ t_{RA} \\ t_{Decl} \end{pmatrix} = \begin{pmatrix} x'_A \\ y'_A \\ x'_B \\ y'_B \end{pmatrix}, \quad (1)$$

where  $x_i, y_i$  is the x-, and y-position of star  $i$  in the HRC image at epoch  $T$  and  $x'_A, y'_A$  are the corresponding optical coordinates of star  $i$ . These coordinates are given by the UCAC3

---

<sup>5</sup>see <http://cxc.harvard.edu/sherpa/bugs/psf.html>

catalog and are corrected for proper motion (see Table 2 and Table 3). We used stars A and B to calculate the transformation and star C to verify the resulting parameters. Multiplying equation 1 with the inverse of the matrix leads to the missing parameters  $t_x$ ,  $t_y$ ,  $r$  and  $\theta$ . The position of RX J0822–4300 at epoch  $T$  can then be calculated straightforwardly by the following equation:

$$\begin{pmatrix} x'_{NS} \\ y'_{NS} \end{pmatrix} = \begin{pmatrix} r \cos \theta & -r \sin \theta \\ r \sin \theta & r \cos \theta \end{pmatrix} \begin{pmatrix} x_{NS} \\ y_{NS} \end{pmatrix} + \begin{pmatrix} t_{RA} \\ t_{Decl} \end{pmatrix}. \quad (2)$$

Calculating the transformation gives a rotation angle  $\theta$  of  $-0.061(31)^\circ$ ,  $0.076(28)^\circ$ ,  $-0.018(27)^\circ$  and  $0.000(29)^\circ$  and a scale factor  $r$  of  $1.00059(60)$ ,  $1.00182(52)$ ,  $1.00044(40)$  and  $1.00033(45)$  for the epochs 1999.97 (HRC-I), 2001.07 (HRC-S), 2005.31 (HRC-I) and 2010.61 (HRC-I), respectively (numbers in parentheses represent the uncertainty in the final digits). The values of  $r$  and  $\theta$  for the HRC-I observations match within the  $1\sigma$  error and are significantly smaller than these for the HRC-S observation.  $t_{RA}$  and  $t_{Decl}$  used in the transformations of the position of RX J0822–4300 from the image- to the world coordinate system are all below  $0.5''$ . Indeed, the largest shift is  $0.29''$  for the y-coordinate in the 2010 HRC-I observation. The positions of the neutron star in the four epochs are listed in Table 4.

To estimate the error in the coordinates of RX J0822–4300, we used the Gaussian elimination algorithm to solve equation 1 for  $t_x$ ,  $t_y$ ,  $r$  and  $\theta$ . We then inserted these parameters into equation 2. This results in equations for  $x'_{NS}$  and  $y'_{NS}$  that depend only on values with known errors:  $x_A$ ,  $y_A$ ,  $x_B$ ,  $y_B$ ,  $x'_A$ ,  $y'_A$ ,  $x'_B$ ,  $y'_B$ ,  $x_{NS}$  and  $y_{NS}$ . The uncertainties in these two neutron star coordinates at each epoch can then be derived through straightforward error propagation:

$$\sigma_{x'_{NS}} = \sqrt{\left(\frac{\partial x'_{NS}}{\partial x_A}\right)^2 \sigma_{x_A}^2 + \left(\frac{\partial x'_{NS}}{\partial y_A}\right)^2 \sigma_{y_A}^2 + \dots + \left(\frac{\partial x'_{NS}}{\partial y_{NS}}\right)^2 \sigma_{y_{NS}}^2} \quad (3)$$

The same formula is applicable for  $\sigma_{y'_{NS}}$ . The corresponding values are listed in parentheses in Table 4.

To check the robustness of our results we applied several cross-checks. We first repeated the transformation using the fiducial points B & C rather than A & B. The positions of RX J0822–4300 obtained this way are also listed in Table 4 for comparison. As can be seen, they have larger errors than using the reference stars A & B (because star C has only a few counts at each epoch) but match the other positions within the  $1\sigma$  uncertainty range. Using the combination of stars A & C rather than A & B leads to large errors, as A and C are located quite close to one another and are in approximately the same direction relative to RX J0822–4300. In a third test we calculated the position of RX J0822–4300 by applying

only a two-dimensional translation of the four images. We weighted the shifts of the three reference stars inversely as the variance and calculated their mean for every epoch. The results for the position of RX J0822–4300 differ for the HRC-I observations by at most 0.4 pixel from the ones calculated according to equation 1. For the HRC-S image the difference in  $x$  is  $\approx 1$  pixel, though this is mainly due to systematic offsets between the HRC-S and HRC-I detectors. This is also seen if we compare the scale factors and rotation angles which we computed for the HRC-I and HRC-S observations.

### 2.3. The Proper Motion of RX J0822–4300

To measure the proper motion of RX J0822–4300 over a baseline of 3886 days we used all four positions obtained from the observations between 1999.97 and 2010.61 and fitted a linear function to  $x'_{NS}(T)$  and  $y'_{NS}(T)$  separately:

$$x'_{NS}(T) = \mu_x T + const_x, \quad (4)$$

$$y'_{NS}(T) = \mu_y T + const_y. \quad (5)$$

In these fits the projected proper motion coordinates  $\mu_x$  and  $\mu_y$  were taken as free parameters for which we find  $\mu_{RA} = -64 \pm 12 \text{ mas yr}^{-1}$  and  $\mu_{Decl} = -31 \pm 13 \text{ mas yr}^{-1}$ , implying a total proper motion of  $\mu_{Tot} = 71 \pm 12 \text{ mas yr}^{-1}$ . For the position angle we find  $244 \pm 11$  degrees, in excellent agreement with the position angle of 243 degrees as implied by the location of the optical expansion center (Winkler et al. 1988). The corresponding transverse space velocity for RX J0822–4300 is  $(672 \pm 115)d_2 \text{ km s}^{-1}$ , scaled relative to a distance of  $d_2 = d/2 \text{ kpc}$ .

Figure 2 shows the actual data for RX J0822–4300 at the three HRC-I epochs, after alignment to a common coordinate system, and Figure 3 shows the progression of RX J0822–4300 and the linear fit to its positions as measured by *Chandra*.

## 3. Discussion

### 3.1. Kinematics and Age

Even though RX J0822–4300 is not moving as fast as previously thought, its association with a supernova remnant of well-constrained age and reasonably well-localized explosion center (Winkler et al. 1988) makes it worthwhile to reexamine the implications of the revised velocity on explosion kinematics and dynamics. The reduced space velocity of the neutron

star means a proportionately smaller momentum. Assuming a typical neutron star mass of  $1.4M_{\odot}$ , its momentum is  $\sim 2 \times 10^{41} \text{ g cm s}^{-1}$ , roughly a factor of 2 smaller than the estimate in WP07. That paper compared the momentum of the neutron star with that of the optical filaments moving in the opposite direction at approximately  $1500 \text{ km s}^{-1}$ . Assuming a typical knot mass of  $0.04M_{\odot}$ , the momentum per knot in the direction opposite the neutron star is  $\sim 1.2 \times 10^{41} \text{ g cm s}^{-1}$ . The momentum of the neutron star would thus be balanced by about 16 such knots, which roughly corresponds to the number known. Thus, to the degree of accuracy to which the filament mass can be inferred, a momentum balance is thus still feasible.

More drastic is the reduction of the estimate of the kinetic energy carried by the stellar remnant:  $6.5 \times 10^{48} \text{ ergs}$ , only a quarter of that estimated in WP07. This corresponds to only 0.6 percent of the nominal  $10^{51} \text{ ergs}$  produced in a canonical core-collapse supernova explosion. This reduced value undoubtedly poses less of a challenge for supernova models. In fact, a potential discrepancy pointed out in WP07 is resolved. The explosion model of Burrows et al. (2007) predicts a kick velocity

$$V_k \sim 1000 \left( \frac{E}{10^{51} \text{ ergs}} \right) \sin \alpha \text{ km s}^{-1}, \quad (6)$$

where  $E$  represents the explosion energy, and  $\sin \alpha$  a parameterization of the explosion anisotropy. For the previous tangential velocity value, even for the most extreme values of anisotropy, corresponding to  $\sin \alpha \sim 1$ , the explosion energy needed to be higher than the canonical  $10^{51} \text{ ergs}$ . With the new, reduced tangential velocity, a range of values of  $\sin \alpha = 0.6$  to  $0.8$  is consistent with the explosion producing Puppis A having an energy of  $10^{51} \text{ ergs}$ . Interestingly, this range of  $\sin \alpha$  indicates a highly asymmetric explosion.

The revised proper motion also has mild implications regarding the age of Puppis A. The proper motions of the optical filaments point back to a common location at RA (2000.) =  $08^{\text{h}}22^{\text{m}}27^{\text{s}}.5$ ; Decl (2000.) =  $-42^{\circ}57'29''$ ; presumably the site of the explosion (Winkler et al. 1988). If no deceleration is assumed, then the remnant age inferred from the filament motion is  $3700 \pm 300$  years. The path of the neutron star, projected backward in time, passes directly through the elliptical region in which the explosion center is likely to have occurred, with a distance of  $371 \pm 31$  arc seconds between the current neutron star location and the nominal explosion center. Using the new proper motion measurement of  $71 \pm 12 \text{ mas yr}^{-1}$ , we find that if the neutron star was born within the optically-defined explosion location, its age should be  $5200 \pm 1000$  years. The age inferred from the neutron star and filament motions can be considered as two independent measurements of the same quantity. They average to  $4450 \pm 750$  years for the age of Puppis A, slightly older than the age of 3700 years based on the optical proper motions alone.

### 3.2. Implications for the Kick Mechanism

While the velocity of RX J0822–4300 is not as extreme as previously thought, it is still high, though more consistent with other fast moving neutron stars (e.g., Hobbs et al. 2005). In light of this new proper motion measurement we briefly reconsider the implications for kick mechanisms. As discussed in WP07, electromagnetically driven or neutrino/magnetic field driven mechanisms generally are not capable of providing a kick velocity in excess of  $500 \text{ km s}^{-1}$ . Even with the lower velocity, these mechanisms are thus unlikely to be applicable to RX J0822–4300. Hydrodynamic recoil mechanisms are the only ones capable of providing a sufficient kick. In fact, recent 2D and 3D simulations (e.g., Scheck et al. 2004, 2006; Wongwathanarat et al. 2010; Nordhaus et al. 2012) suggest that kick velocities higher than  $\sim 500 \text{ km s}^{-1}$  are easily induced by hydrodynamically driven mechanisms after about 1 second of post-bounce evolution during core collapse. In these hydrodynamical explosion models the gravitational pull of slow-moving ejecta in front of the neutron star can – during the first seconds of the explosion – continue to accelerate it to considerably higher velocities.”

Strong independent evidence supporting a hydrodynamic kick mechanism for RX J0822–4300 comes from the implications associated with the discovery and the modeling of its pulsations. Gotthelf & Halpern (2009) discovered a period of 112 ms in RX J0822–4300. This periodicity had been missed by prior investigators because of an abrupt 180-degree phase change of the pulse profile at about 1.2 keV. The period and the very small period derivative imply a surface magnetic field strength of  $\lesssim 9.8 \times 10^{11} \text{ G}$  and a spindown age of larger than  $2.2 \times 10^5 \text{ yr}$ . The very low magnetic field gives rise to the attribution of “antimagnetar” to this object. Energy- and pulse-phase resolved spectroscopy led to a model that reproduces the observed properties. The model consists of two antipodal hotspots, modeled by blackbodies whose crossover in flux corresponds to the energy at which the phase reverses. The angles from the hot spot to the pole and from the line of sight to the rotation axis are degenerate; one has a value of  $86^\circ$ , the other a value of  $6^\circ$  (Gotthelf et al. 2010). Interestingly, the model degeneracy allows either for the spin axis to be parallel with the direction of motion, or for the spin and kick directions to be maximally misaligned.

The two most constraining aspects of these results on possible kick models are the low magnetic field and the initial spin period. Models invoking magnetic processes require the nascent neutron star to have a high magnetic field and/or high initial spin periods (Lai 2001). As pointed out in Gotthelf & Halpern (2009), the only current models satisfying these new constraints are the hydrodynamical ones that potentially produce very high velocities. Thus despite the less restrictive, lower inferred space velocity of RX J0822–4300, the conclusion of WP07 regarding likely ejection mechanisms still holds.

The solution that favors spin-kick alignment is supported circumstantially by the fact

that such alignment is observed in a number of neutron stars (e.g., Figure 5 in Wang et al. 2007). More specific support from within Puppis A comes from the alignment of HI cavities, which presumably represent the path of jets from the initial explosion, along the direction of motion of the neutron star (Reynoso et al. 2003). Further, comparison of numerical simulations with the distribution of pulsars with known spin-kick angles suggests that the observed spin-kick distribution requires the initial spin period to be shorter than the kick timescale (Wang et al. 2007). Since the hydrodynamic recoil time scale ( $\gtrsim 1$  s) is considerably longer than the 112 ms pulsation period, one might reasonably expect spin-kick alignment in RX J0822–4300.

#### 4. Summary

Two previous proper motion measurements of RX J0822–4300, incorporating the same *Chandra* HRC data sets, produced discrepant results. HB06 found a proper motion of  $104 \pm 35$  mas yr<sup>-1</sup> at a position angle of  $240^\circ \pm 28^\circ$ . WP07, using a different analysis approach, found a considerably higher value of  $165 \pm 25$  mas yr<sup>-1</sup> at a position angle of  $248^\circ \pm 14^\circ$ . A combined analysis, incorporating a new deep observation and a total time baseline twice as long as was available previously, yields an improved value that is smaller than either of the two published numbers, but at a position angle consistent with both. We now find with high confidence a value for the proper motion of  $71 \pm 12$  mas yr<sup>-1</sup> at a position angle of  $244^\circ \pm 11^\circ$ . For an assumed distance to Puppis A of 2 kpc, the proper motion corresponds to a tangential velocity of  $672 \pm 115$  km s<sup>-1</sup>. This smaller velocity eases most challenges that RX J0822–4300 previously posed to pulsar-kick models, but still requires a hydrodynamic kick model in a highly asymmetric explosion. Considering the proper motion based age estimate as a second and independent measurement to the one inferred from the motion of optical filaments, it can be averaged to  $4450 \pm 750$  yrs which implies that Puppis A is slightly older than the 3700 years based on the proper motions of the optical filaments.

#### Acknowledgments

TP acknowledges support by the International Max-Planck Research School on Astrophysics at the Ludwig-Maximilians University, IMPRS; PFW acknowledges support from the NSF through grant AST-0908566. We are grateful to Daniel Patnaude for his contributions in scheduling and setting up the observations and to several members of the Helpdesk staff at the *Chandra* X-ray Center for assistance at various stages of this project, and especially for helping to sort out the troublesome software bug described in §2.1. We also acknowledge the use of the *Chandra* data archive.

## REFERENCES

- Becker, W., X-Ray Emission from Pulsars and Neutron Stars, in *Neutron Stars and Pulsars*, W. Becker, Ed. Berlin, Germany: Springer, 2009, pp. 91-140
- Burrows, A., Hayes, J., & Fryxell, B. A. 1995, *ApJ*, 450, 830
- Burrows, A., Livne, E., Dessart, L., Ott, C. D., & Murphy, J. 2007, *ApJ*, 655, 416
- Camilo, F., Manchester, R. N., Gaensler, B. M., Lorimer, D. R., & Sarkissian, J. 2002, *ApJ*, 567, L71
- Caraveo, P. A. 1993, *ApJ*, 415, L111+
- Chakrabarty, D., Pivovarov, M. J., Hernquist, L. E., Heyl, J. S., & Narayan, R. 2001, *ApJ*, 548, 800
- Cutri, R.M., Skrutskie, M.F., van Dyk, S., et al., 2003, *The 2MASS All-Sky Catalog of Point Sources*, University of Massachusetts and Infrared Processing and Analysis Center (IPAC/California Institute of Technology)
- Frail, D. A., Goss, W. M., & Whiteoak, J. B. Z. 1994, *ApJ*, 437, 781
- Gotthelf, E. V., & Halpern, J. P. 2009, *ApJ*, 695, L35
- Gotthelf, E. V., Perna, R., & Halpern, J. P. 2010, *ApJ*, 724, 1316
- Hobbs, G., Lorimer, D. R., Lyne, A. G., & Kramer, M. 2005, *MNRAS*, 360, 974
- Hughes, J. P., Slane, P. O., Burrows, D. N., Garmire, G., Nousek, J. A., Olbert, C. M., & Keohane, J. W. 2001, *ApJ*, 559, L153
- Hui, C.Y., & Becker, W., 2006, *A&A*, 457, L33
- Lai, D. 2001, *LNP Vol. 578: Physics of Neutron Star Interiors*, 578, 424
- Nordhaus, J., et al., *MNRAS*, in press
- Petre, R., Becker, C. M., & Winkler, P. F. 1996, *ApJ*, 465, L43+
- Reynoso, E. M., Green, A. J., Johnston, S., Dubner, G. M., Giacani, E. B., & Goss, W. M. 2003, *MNRAS*, 345, 671
- Scheck, L., Kifonidis, K., Janka, H. Th., Müller, E., 2006, *A&A*, 457, 963

- Scheck, L., Plewa, T., Janka, H. Th., Müller, E., 2004, PhRvL, 92, 011103
- Tananbaum, H. 1999, IAU Circ., 7246, 1
- Wang, C., Lai, D., Han, J.L., 2007, ApJ, 656,399
- Winkler, P.F., Petre, R., 2007, ApJ, 670, 635
- Winkler, P.F., Tuttle, J.H., Kirshner, R.P., Irwin, M.J., 1988, in IAU Colloq. 101: Supernova Remnants and the Interstellar Medium, eds. R.S. Roger & T.L. Landecker, 65
- Wongwathanarat, A., Janka, H. Th., Müller, E., 2010, ApJ, 725, 106
- Zacharias, N., Finch, C., Girard, T., et al., 2009, UCAC3 Catalog (VizieR On-line Data Catalog I/315)

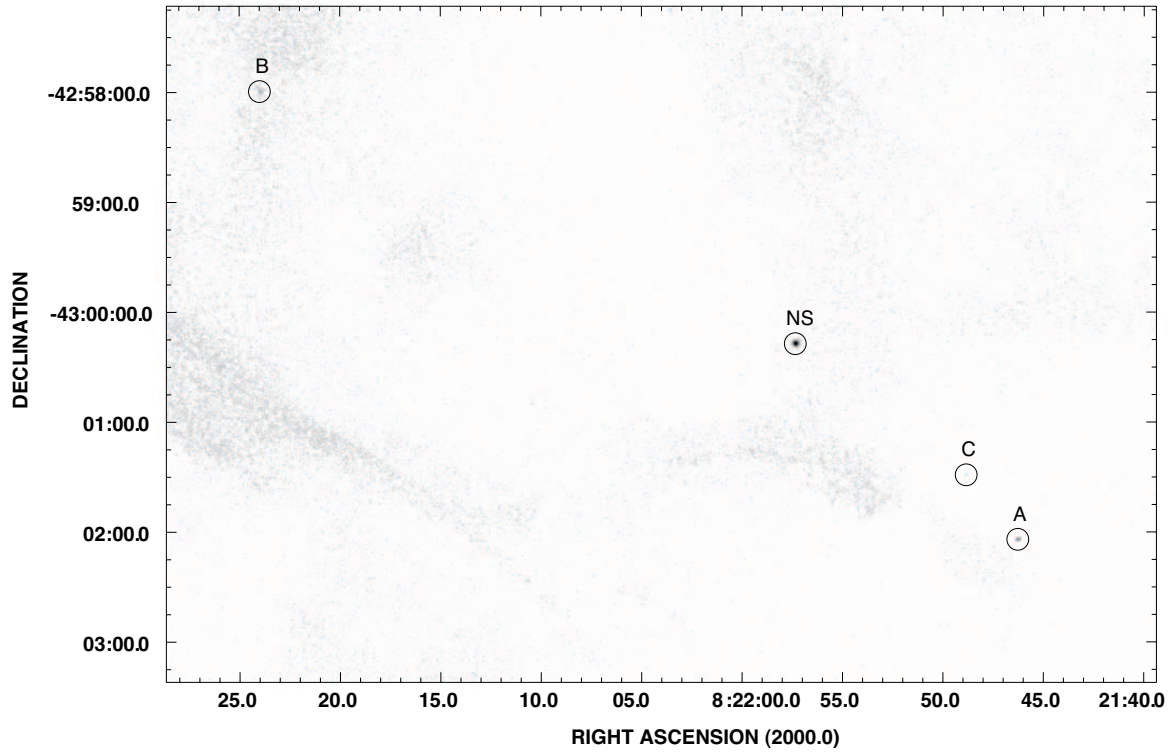


Fig. 1.— The 2010 epoch *Chandra* HRC-I image with reference sources and RX J0822–4300 marked by circles. NS marks the position of RX J0822–4300; A, B and C that of the fiducial stars used as local calibrators for absolute astrometry. The field measures 6 by 9 arcmin and is oriented north up, east left.

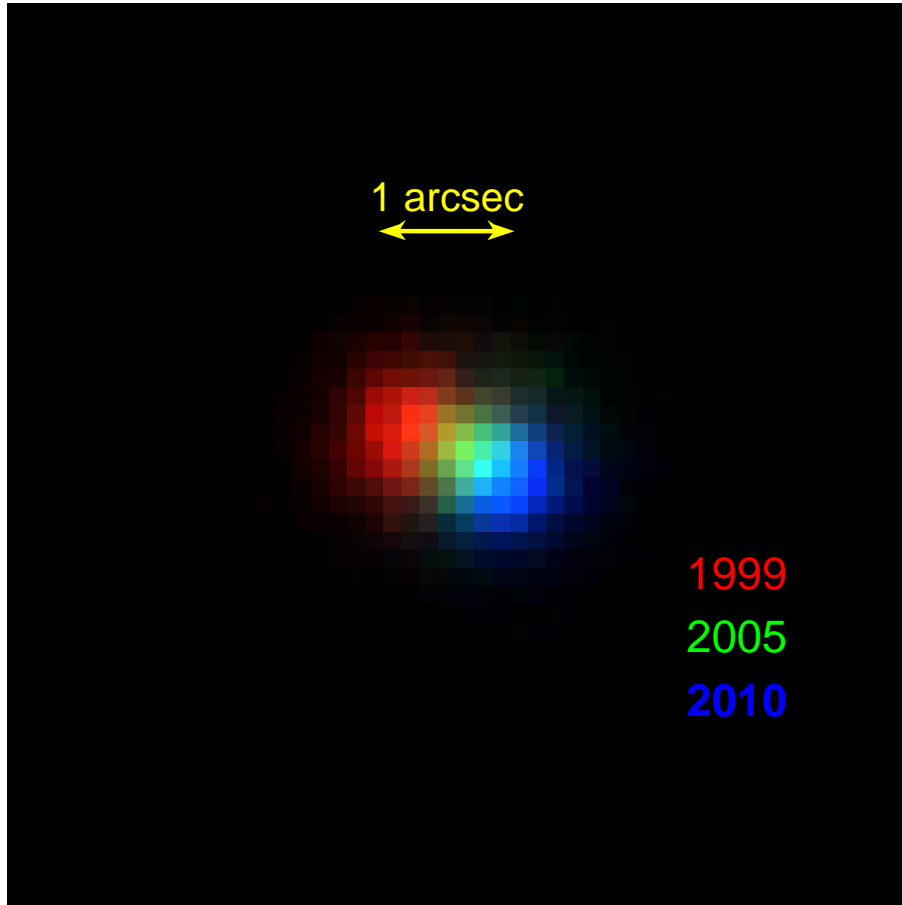


Fig. 2.— This enlargement of the immediate region of RX J0822–4300 shows the data from all three HRC-I epochs (after alignment to a common coordinate system) in different colors. The neutron star’s motion is apparent.

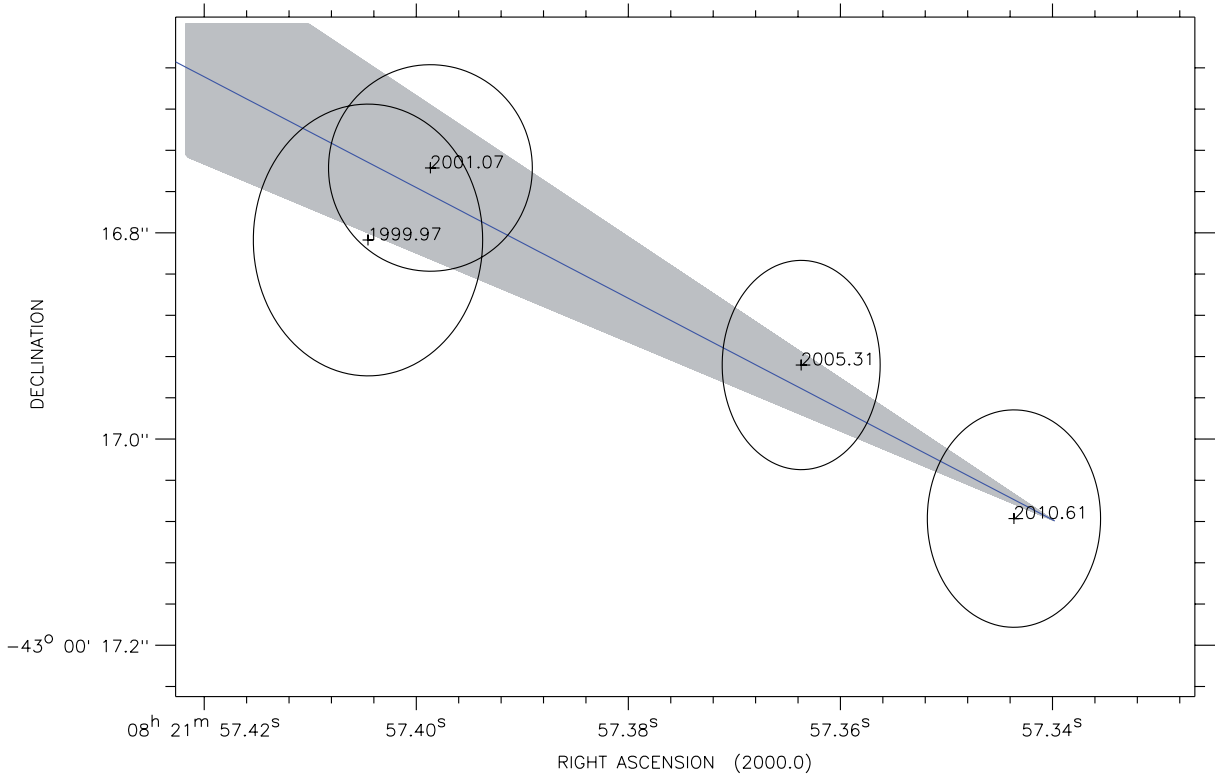


Fig. 3.— Position of RX J0822–4300 as measured at four epochs over a baseline of 3886 days, showing the proper motion from upper left (NE) to lower right (SW). The  $1\sigma$  position uncertainty at each epoch is indicated, and the observation dates are labeled. The gray shaded bar depicts the direction toward the remnant’s optical expansion center, i.e. toward the birthplace of RX J0822–4300. The straight blue line indicates the CCO’s proper motion path as fitted from the four positions.

Table 1. *Chandra* observations of the neutron star in Puppis A

Instrument	ObsId	Date (MJD)	ONTIME (sec)	Exposure Time (sec)
HRC-I	749	21/22 Dec 1999 (51533)	18014	9907
HRC-S	1859	25 Jan 2001 (51934)	19667	19524
HRC-I	4612	25 Apr 2005 (53485)	40165	21410
HRC-I	11819	10/11 Aug 2010 (55418)	33681	15509
HRC-I	12201	11 Aug 2010 (55419)	38680	17855

Table 2. Position, proper motion and angular distance of astrometric reference stars near RX J0822–4300 as listed in the UCAC3 catalog (Zacharias et al. 2009).

Designation		Position (J2000.0)		Proper Motion		$\delta d$
Short	3UCAC	R.A.	Decl.	$\mu_{R.A.}$	$\mu_{Decl.}$	arcmin
		(h m s)	(d m s)	mas yr <sup>-1</sup>	mas yr <sup>-1</sup>	
A	094-058669	08 21 46.292(1)	-43 02 03.64(5)	$-14.3 \pm 2.0$	$-3.6 \pm 5.5$	2.8
B	095-060051	08 22 24.003(3)	-42 57 59.37(2)	$0.0 \pm 4.0$	$10.2 \pm 2.0$	5.3
C	094-058675	08 21 48.876(6)	-43 01 28.33(6)	$-55.4 \pm 8.6$	$2.0 \pm 6.1$	2.0

Note. —  $1\sigma$  uncertainty of the last digit in parentheses

Table 3. Properties of the astrometric reference stars

ObsID	Epoch	Source	X-ray <sup>a</sup>		Counts	Rate cts/ks	Optical <sup>a</sup>	
			R.A. (h m s)	Decl. (d m s)			R.A. (h m s)	Decl. (d m s)
749	1999.97	NS	08 21 57.411(01)	-43 00 16.63(01)	2544	257.0		
		A	08 21 46.295(10)	-43 02 03.26(17)	46	4.6	08 21 46.292(01)	-43 02 03.64(02)
		B	08 22 24.008(25)	-42 57 59.58(17)	46	4.7	08 22 24.003(03)	-42 57 59.37(04)
		C	08 21 48.874(18)	-43 01 28.13(26)	13	1.3	08 21 48.876(06)	-43 01 28.33(09)
1851	2001.07	NS	08 21 57.390(01)	-43 00 16.91(01)	5005	256.5		
		A	08 21 46.316(09)	-43 02 03.77(11)	70	3.6	08 21 46.291(01)	-43 02 03.64(02)
		B	08 22 23.930(21)	-42 57 59.38(20)	139	7.1	08 22 24.003(03)	-42 57 59.36(04)
		C	08 21 48.880(17)	-43 01 28.62(28)	11	0.5	08 21 48.870(07)	-43 01 28.33(09)
4612	2005.31	NS	08 21 57.374(01)	-43 00 17.07(01)	5596	261.6		
		A	08 21 46.297(08)	-43 02 03.70(08)	91	4.3	08 21 46.285(02)	-43 02 03.66(05)
		B	08 22 24.006(11)	-42 57 59.60(23)	57	2.7	08 22 24.003(04)	-42 57 59.31(05)
		C	08 21 48.881(22)	-43 01 28.40(26)	7	0.3	08 21 48.849(10)	-43 01 28.32(11)
11819/12201	2010.61	NS	08 21 57.329(01)	-43 00 17.38(01)	9152	274.7		
		A	08 21 46.268(08)	-43 02 03.93(07)	132	4.0	08 21 46.279(03)	-43 02 03.68(08)
		B	08 22 23.979(13)	-42 57 59.60(23)	96	2.9	08 22 24.003(07)	-42 57 59.26(06)
		C	08 21 48.853(22)	-43 01 28.68(17)	21	0.6	08 21 48.822(14)	-43 01 28.31(15)

Note. — <sup>a</sup>1  $\sigma$  uncertainty of the last two digits in parentheses

Table 4. Positions of RX J0822–4300

Epoch	Ref. Stars	R.A. (h m s)	Decl. (d m s)
1999.97	A & B	08 21 57.403(11)	-43 00 16.80(13)
	B & C	08 21 57.409(16)	-43 00 16.72(21)
2001.07	A & B	08 21 57.398(10)	-43 00 16.74(10)
	B & C	08 21 57.403(15)	-43 00 16.65(22)
2005.31	A & B	08 21 57.363(08)	-43 00 16.93(10)
	B & C	08 21 57.349(19)	-43 00 16.92(22)
2010.61	A & B	08 21 57.343(08)	-43 00 17.08(11)
	B & C	08 21 57.312(21)	-43 00 16.99(18)

Note. —  $1\sigma$  position uncertainty in parentheses